Engineered nanomedicine for myeloma and bone microenvironment targeting

Archana Swami[a,1], Michaela R. Reagan[b,1], Pamela Basto[c], Yuji Mishima[b], Nazila Kamaly[a], Siobhan Glavey[b], Sufeng Zhang[c], Michele Moschetta[b], Dushanth Seevaratnam[a], Yong Zhang[b], Jinhe Liu[a], Masoumeh Memarzadeh[b], Jun Wu[a], Salomon Manier[b], Jinjun Shi[a], Nicolas Bertrand[c], Zhi Ning Lu[b], Kenichi Nagano[d], Roland Baron[d], Antonio Sacco[b], Aldo M. Roccaro[b], Omid C. Farokhzad[a,e,2], and Irene M. Ghobrial[b,2]

[a]Laboratory of Nanomedicine and Biomaterials, Department of Anesthesiology, Brigham and Women's Hospital, Harvard Medical School, Boston, MA 02115; [b]Department of Medical Oncology, Dana-Farber Cancer Institute, Harvard Medical School, Boston, MA 02115; [c]The David H. Koch Institute for Integrative Cancer Research, Massachusetts Institute of Technology, Cambridge, MA 02139; [d]Department of Oral Medicine, Infection and Immunity, Harvard School of Dental Medicine, Harvard Medical School, Boston, MA 02115; and [e]King Abdulaziz University, Jeddah, Saudi Arabia

Edited by Robert Langer, Massachusetts Institute of Technology, Cambridge, MA, and approved May 30, 2014 (received for review January 21, 2014)

Bone is a favorable microenvironment for tumor growth and a frequent destination for metastatic cancer cells. Targeting cancers within the bone marrow remains a crucial oncologic challenge due to issues of drug availability and microenvironment-induced resistance. Herein, we engineered bone-homing polymeric nanoparticles (NPs) for spatiotemporally controlled delivery of therapeutics to bone, which diminish off-target effects and increase local drug concentrations. The NPs consist of poly(D,L-lactic-co-glycolic acid) (PLGA), polyethylene glycol (PEG), and bisphosphonate (or alendronate, a targeting ligand). The engineered NPs were formulated by blending varying ratios of the synthesized polymers: PLGA-*b*-PEG and alendronate-conjugated polymer PLGA-*b*-PEG-Ald, which ensured long circulation and targeting capabilities, respectively. The bone-binding ability of Ald-PEG-PLGA NPs was investigated by hydroxyapatite binding assays and ex vivo imaging of adherence to bone fragments. In vivo biodistribution of fluorescently labeled NPs showed higher retention, accumulation, and bone homing of targeted Ald-PEG-PLGA NPs, compared with nontargeted PEG-PLGA NPs. A library of bortezomib-loaded NPs (bone-targeted Ald-Bort-NPs and nontargeted Bort-NPs) were developed and screened for optimal physiochemical properties, drug loading, and release profiles. Ald-Bort-NPs were tested for efficacy in mouse models of multiple myeloma (MM). Results demonstrated significantly enhanced survival and decreased tumor burden in mice pretreated with Ald-Bort-NPs versus Ald-Empty-NPs (no drug) or the free drug. We also observed that bortezomib, as a pretreatment regimen, modified the bone microenvironment and enhanced bone strength and volume. Our findings suggest that NP-based anticancer therapies with bone-targeting specificity comprise a clinically relevant method of drug delivery that can inhibit tumor progression in MM.

targeting nanomedicine | alendronate-PLGA-PEG | bone metastasis | bisphosphonate

The incidence of bone metastasis is common in 60–80% of cancer patients (1). During bone metastasis, cancer cells induce a sequence of changes in the microenvironment such as secreting cytokines to increase the activity of osteoclasts via the parathyroid hormone-related protein (PTHrP), receptor activator of nuclear factor-κB ligand (RANKL), and interleukin-6 (IL-6), resulting in increased bone resorption and secretion of growth factors from the bone matrix (2). This creates a "vicious cycle" of bone metastasis, where bone marrow becomes packed with cancer cells that develop resistance to conventional chemotherapy, and leads to devastating consequences of bone fractures, pain, hypercalcaemia, and spinal cord and nerve compression syndromes (2, 3). Multiple myeloma (MM) is a plasma cell cancer that proliferates primarily in bone marrow and causes osteolytic lesions (1). Antiresorption agents, such as bisphosphonates, may alleviate bone pain, but they are ineffective at inducing bone healing or osteogenesis in MM patients (4).Bortezomib is a proteasome inhibitor that has shown marked antitumor effects in patients with MM. Proteasome inhibitors, such as bortezomib, are also effective at increasing bone formation, both preclinically and clinically (5–9). However, the major drawback of bortezomib use in early stages of MM development is its toxicity, specifically, peripheral neuropathy (5). Therefore, we aimed to develop a method to deliver bortezomib with decreased off-target side effects by using bone-specific, bortezomib-loaded nanoparticles (NPs). The NP system was based on biodegradable, biocompatible, and Food and Drug Administration (FDA)-approved components, which are both clinically and translationally relevant. NPs derived from poly(D,L-lactic-co-glycolic acid) (PLGA), a controlled release polymer system, are an excellent choice because their safety in the clinic is well established (10, 11). Polyethylene glycol (PEG)-functionalized

Significance

Limited treatment options exist for cancer within the bone, as demonstrated by the inevitable, pernicious course of metastatic breast, prostate, and blood cancers. The difficulty of eliminating bone-residing cancer necessitates novel, alternative treatments to manipulate the tumor cells and their microenvironment, with minimal off-target effects. To this end, we engineered bone-homing, stealth nanoparticles to deliver anticancer, bone-stimulatory drugs, and demonstrated their utility with bortezomib (a model drug) and multiple myeloma (a model cancer). To test our hypothesis that increasing bone volume and strength inhibits tumor growth, mice were treated with these nanoparticles before being injected with cancer cells. Results demonstrated significantly slower myeloma growth and prolonged survival. Our research demonstrates the potential of bone-homing nanomedicine as an efficacious cancer treatment mechanism.

Author contributions: A. Swami, M.R.R., O.C.F., and I.M.G. designed research; A. Swami, M.R.R., P.B., Y.M., N.K., S.G., S.Z., M. Moschetta, D.S., Y.Z., J.L., M. Memarzadeh, J.W., S.M., J.S., N.B., Z.N.L., K.N., R.B., A. Sacco, and A.M.R. performed research; A. Swami, M.R.R., R.B., A.M.R., O.C.F., and I.M.G. analyzed data; and A. Swami, M.R.R., P.B., N.K., O.C.F., and I.M.G. wrote the paper.

Conflict of interest statement: I.M.G. discloses her Advisory Board Membership with Novartis, Onyx, and BMS. O.C.F. discloses his financial interest in BIND Therapeutics, Selecta Biosciences, and Blend Therapeutics, three biotechnology companies developing nanoparticle technologies for medical applications. BIND, Selecta, and Blend did not support the aforementioned research, and currently these companies have no rights to any technology or intellectual property developed as part of this research.

This article is a PNAS Direct Submission.

Freely available online through the PNAS open access option.

[1]A.S. and M.R.R. contributed equally to this work.

[2]To whom correspondence may be addressed. Email: ofarokhzad@zeus.bwh.harvard.edu or irene_ghobrial@dfci.harvard.edu.

This article contains supporting information online at www.pnas.org/lookup/suppl/doi:10.1073/pnas.1401337111/-/DCSupplemental.

PLGA NPs are especially desirable as PEGylated polymeric NPs have significantly reduced systemic clearance compared with similar particles without PEG (12, 13). A number of FDA-approved drugs in clinical practice use PEG for improved pharmaceutical properties such as enhanced circulation in vivo (12, 13). To target NPs to bone [rich in the mineral hydroxyapatite (HA)], the calcium ion-chelating molecules of bisphosphonates represent a promising class of ligands (14). Bisphosphonates, upon systemic administration, are found to deposit in bone tissue, preferentially at the high bone turnover sites, such as the metastatic bone lesions, with minimal nonspecific accumulation (14) and were used herein to deliver NPs to the bone.

A few systems explored for MM treatment have been tested in vitro including the following: (*i*) snake venom and silica NPs (15); (*ii*) thymoquinone and PLGA-based particles (16); (*iii*) curcumin and poly(oxyethylene) cholesteryl ether (PEG-Chol) NPs (17), polyethylenimine-based NPs for RNAi in MM (18), paclitaxel-Fe_3O_4 NPs (19), and liposomes (20). However, none of the above-mentioned systems have aimed to manipulate the bone marrow microenvironment rather than the myeloma cells directly (21). To date, there are no reports of using bone-targeted, controlled release, polymeric NPs with stealth properties for MM therapy. In this study, we designed NPs bearing three main components: (*i*) a targeting element that can selectively bind to bone mineral; (*ii*) a layer of stealth (PEG) to minimize immune recognition and enhance circulation; and (*iii*) a biodegradable polymeric material, forming an inner core, that can deliver therapeutics and/or diagnostics in a controlled manner. In this study, the physicochemical properties of a range of NPs was investigated (including NP size, charge, targeting ligand density, drug loading, and drug release kinetics) and an optimal formulation with ideal properties and maximal drug encapsulation was used for in vivo efficacy studies. We fine-tuned the NP targeting ligand density to optimize its bone-binding ability and further investigated its application for targeting myeloma in the bone microenvironment. We believe our NP system has the potential to increase drug availability by improving pharmacokinetics and biodistribution that can provide bone microenvironment specificity, which may increase the therapeutic window and most certainly decrease the off-target effects (12, 13).

Results and Discussion

Design, Synthesis, and Characterization of Alendronate-PEG-PLGA NPs. The design and synthesis of alendronate-PEG-PLGA (Ald-PP), bone-targeted NPs engineered with fine-tuned Ald density on their surface, and nontargeted PEG-PLGA (PP) NPs, are shown in Fig. 1 *A* and *B* and Fig. S1. The physicochemical characteristics and bortezomib drug load of the NPs (Fig. 1 *C* and *D*) were optimized by analyzing a library of NPs formulated (Fig. S2) with varying parameters such as the following: formulation technique, polymer molecular weight, polymer concentration, ratio of organic to aqueous phase, formulation condition, and initial drug feed (Fig. 1*D* and Fig. S2 *C*–*E*). The lead candidate NPs synthesized by single-emulsion method of formulation had optimal sizes in the range of 150–200 nm and nearly neutral to slightly negative ζ potentials (Fig. 1 *C* and *D*, and Fig. S2*C*), and were further standardized to enhance their drug load. To obtain optimal binding to the bone mineral along with maximum stealth properties, we blended varying ratios of the polymers: PLGA-*b*-PEG-Ald (Fig. S1) and PLGA-*b*-PEG for NP formulation (Fig. 1 *A*, *B*, *E*, and *F*). Different ratios of blended polymers altered the Ald content of NPs. We analyzed the stability and size of these NPs in the presence of ions and serum conditions, and the results demonstrated time-dependent increase in NP size, when the content of PLGA-*b*-PEG-Ald polymer in the NPs was higher than 20% (Fig. 1*F*). Thus, it is important to optimize the Ald content of NPs for effective bone binding with maintenance of stealth properties, which ensures enhanced bone homing of NPs, in vivo.

Encapsulation and Release of Bortezomib from NPs. The ability of the NPs to encapsulate high loads of drug and subsequently release the drug in a controlled manner was significantly affected by PLGA molecular weight and content in the NPs, in addition to the formulation techniques and conditions, as investigated by using HPLC. In the case of NPs formulated by the solvent dispersion method, the hydrodynamic diameter (dynamic light

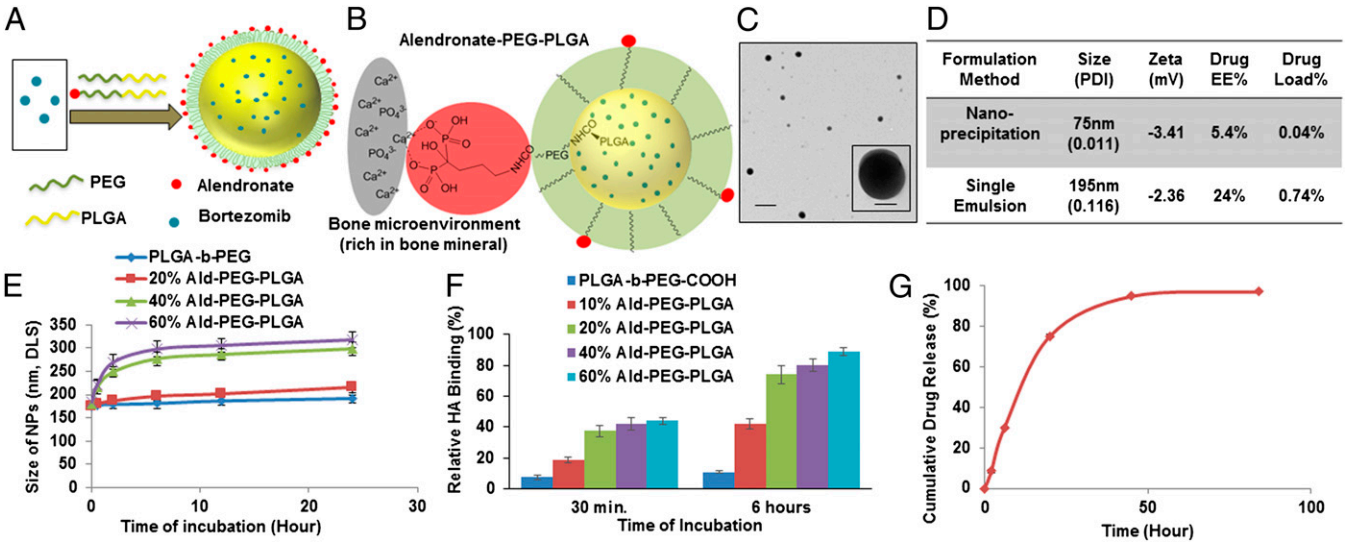

Fig. 1. Design, engineering, and characterization of NPs for bone targeting. (*A*) Schematic illustration of alendronate-conjugated PEG-PLGA (Ald-PP) NPs synthesized by blending polymers (PLGA-*b*-PEG-Ald and PLGA-*b*-PEG) in varying ratios and encapsulating the drug bortezomib. (*B*) Schematic representation of the mechanism of affinity of Ald-PP NPs with bone mineral (gray, bone mineral; red, Ald; green, PEG; yellow, PLGA). (*C*) Representative TEM image of Ald-PP NPs (single emulsion), negatively stained, imaged at 80.0 kV. (Scale bars: 500 nm; *Inset*, 100 nm.) (*D*) Physiochemical characteristics of Ald-PP NPs. (*E*) Size of the Ald-PP NPs (single emulsion) with varying content of polymer PLGA-*b*-PEG-Ald, in presence of serum, with time. (*F*) Quantitative evaluation of HA binding of NPs (single emulsion) with varying content of PLGA-*b*-PEG-Ald polymer. PLGA-*b*-PEG (-COOH terminated) polymeric NPs were used as control. (*G*) Release kinetics of encapsulated drug bortezomib from the Ald-PP NPs (single emulsion), in physiological ionic and temperature conditions.

scattering) was small (80–100 nm), with lower encapsulation efficiency (5–8%) along with lower drug loading (0.04–0.09%). In the case of the single-emulsion NPs with optimal polymer weight (M_r, 45 kDa) and formulation conditions, the NP drug load was enhanced 16- to 20-fold and the release kinetics showed sustained drug release (Fig. 1 *D* and *G*, and Fig. S2 *B*, *D*, and *E*). This can be attributed to the dispersion of the encapsulated drug from the PLGA core of NP by diffusion and polymer degradation. The NPs protect the drug from the external environment, and increase its blood circulation time, thereby increasing the drug content at the target site.

In Vitro Bone Targeting of NPs. Bone microenvironment is rich in HA, particularly the sites of metastatic lesions, where the bone turnover is high, and to investigate the bone affinity of the Ald-PP NPs (single emulsion), we performed the HA binding assay (Fig. 1*F*), in comparison with nontargeted PP NPs (Fig. 2*A*). The Ald-PP NP solution on incubation with HA in any form (NPs, microparticles, or bone chips) showed immediate binding (Figs. 1*F* and 2 *B*–*D*). The results demonstrated a significant rise in the HA binding of NPs as the content of PLGA-*b*-PEG-Ald polymer in the NPs was increased from 0% to 20%. This trend plateaued on further increase of PLGA-*b*-PEG-Ald polymer content in NPs to 40% or 60% (Fig. 1*F*). Thus, optimized, targeted Ald-PP NPs with effective HA binding had 20% PLGA-*b*-PEG-Ald polymer, for all studies thereafter. The HA affinity of targeted NPs was also confirmed by the following: transmission electron microscopy (TEM) using HA in NP form (Fig. 2*B*); scanning electron microscopy (SEM) using HA generated from simulated body fluid (Fig. 2*C*); and fluorescence microscopy using bone fragments (mice skull bone, ex vivo) with fluorescently labeled NPs (Fig. 2*D*). Nontargeted PP NPs did not show any specificity or binding to HA, in any form (Fig. 2 *B*–*D*). These results confirmed the impact of the design of our engineered targeted NPs in bone mineral binding and the differential binding of targeted NPs facilitated the next in vivo experiments.

In Vivo Biodistribution Studies of NPs. The bone-homing ability of targeted Ald-PP NPs (single emulsion) was investigated by conducting biodistribution studies using fluorescently labeled NPs (PLGA-Alexa$_{647}$) tracked with an in vivo imaging system (IVIS) in mice (Fig. 2 *E* and *F*), after i.p. injection. At 24 h, mice injected with targeted NPs showed increased retention in areas of the spleen, femur, spin, skull, and lymph nodes (Fig. 2*E*). The higher retention of targeted NPs compared with nontargeted NPs was confirmed by quantifying the total radiance efficiency of the mice body image (Fig. 2 *G* and *H*). For further examination of the retention and bone-homing ability of targeted NPs, the dissected femur and spine of the mice were sectioned, counterstained with DAPI, and imaged with a fluorescence microscope. Quantification of the NP in bone sections, as measured by the fluorescence (Alexa$_{647}$), revealed 9.6-fold increased accumulation of targeted NPs compared with nontargeted NPs (Fig. 2 *F* and *H*, and Fig. S3). Thus, in vivo biodistribution and histology studies complement the in vitro and ex vivo bone-binding results, which highlight the potential of our engineered NPs for targeting bone.

In Vitro Uptake and Efficacy Studies of NPs in Myeloma Cells. Cellular uptake and accumulation of fluorescently labeled Ald-PP and PP NPs (single emulsion) were quantified using flow cytometry, and demonstrated uptake by peripheral blood mononuclear cells (PBMCs), and to a greater extent by myeloma cells (MM1S) (Fig. 3*A*) with no observable cytotoxic effects. These NPs were also visualized in MM1S cells as demonstrated by using fluorescence microscopy after 24 h of in vitro culture with NPs (Fig. 3*B*). Bortezomib-loaded PP NPs (Bort-NPs) were then assessed for their ability to induce apoptosis and inhibit MM growth in vitro. Apoptosis analysis assessed by Annexin-V/propidium iodide (PI)

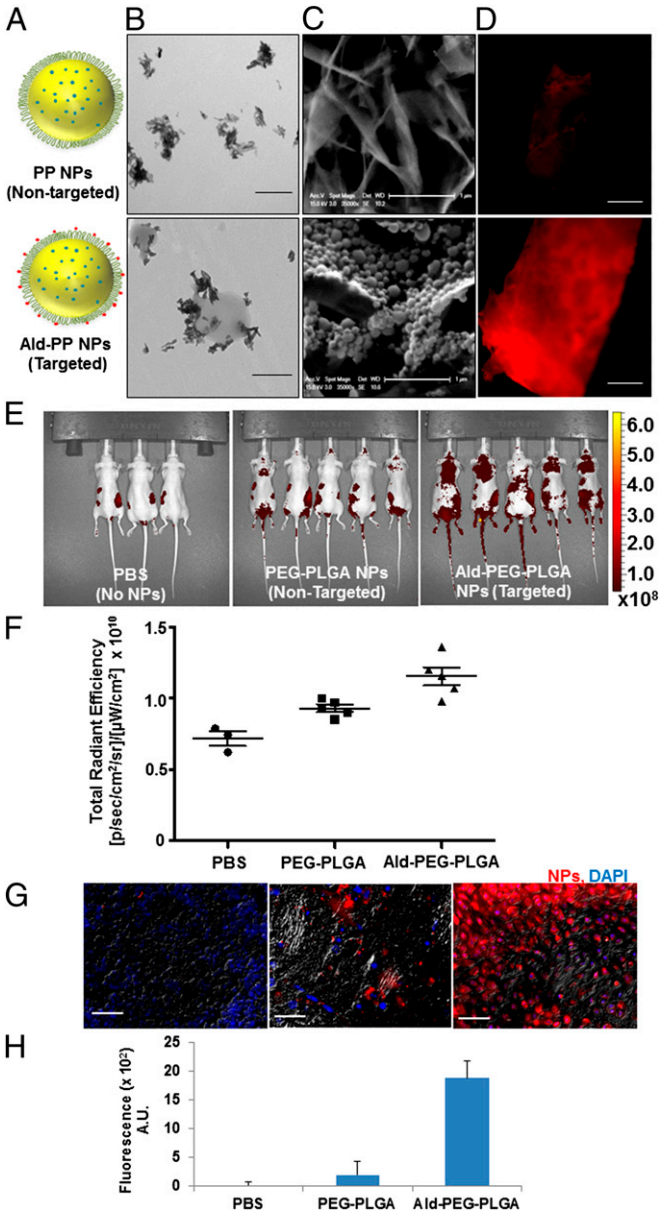

Fig. 2. Bone-targeting ability of Ald-PP NPs (single emulsion). (*A*) Schematic illustration of bone-targeted Ald-PP NPs and nontargeted PP NPs. (*B*) Representative TEM image of Ald-PP (*Lower*) NPs surface interactions with HA rods, which is not observed in case of nontargeted PP NPs (*Upper*). (Scale bar: 500 nm.) (*C*) Representative SEM image of interaction of NPs (targeted Ald-PP: *Lower*; nontargeted PP: *Upper*) with crystalized HA (scale bar: 1 μm) after incubation with NP solution and washing. (*D*) Representative fluorescence image of bone fragment after incubation with fluorescently labeled NP solution (targeted Ald-PP: *Lower*; nontargeted PP: *Upper*) (ex vivo), and washing. (Scale bar: 500 μm.) (*E*) Whole-body mice imaging (IVIS), where targeted NP (*Right*) clearance is compared with nontargeted NPs (*Center*) and PBS (*Left*) (24-h time point, i.p. injection). Scale represents luminescence signal from Alexa$_{647}$-labeled NPs, representing NP biodistribution. (*F*) Total fluorescence quantified in the region of interest of IVIS images from *E*. (*G*) Representative images of bone histology in merged channels (405: DAPI; 647: NPs; and bright field) for PBS (*Left*), nontargeted NPs (*Center*), and targeted NPs (*Right*). (Scale bar: 100 μm.) (*H*) Quantification of NP homing as measured from the bone (femur and spine) histology by fluorescence intensity (average) quantification in the 647 channel in multiple sections of bone, covering entire region representatively, in different mice (n = 3).

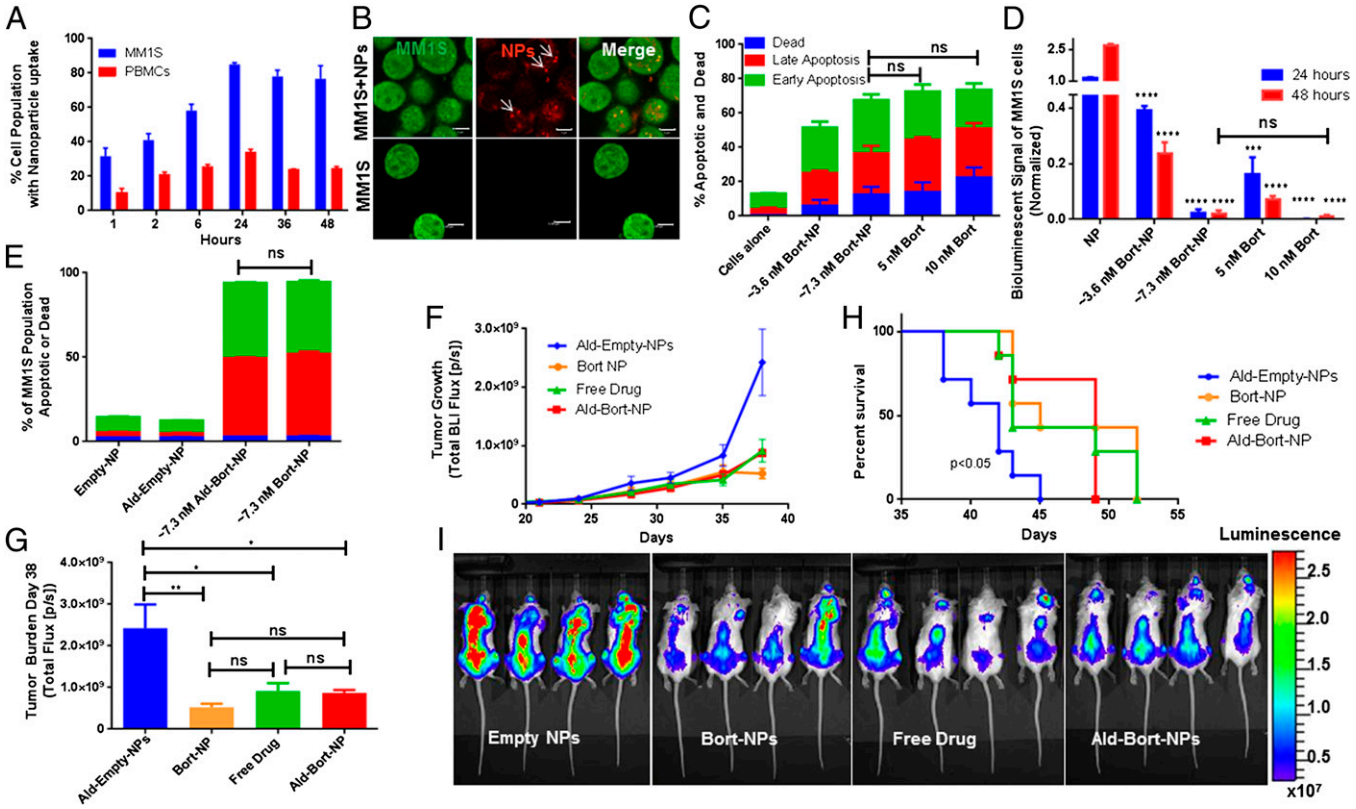

Fig. 3. In vitro and in vivo efficacy of NPs (single emulsion). (*A*) Cellular uptake of NPs during coculture with myeloma (MM1S) cells and peripheral blood mononuclear cells (PBMCs). (*B*) $Alexa_{647}$-labeled NPs imaged in GFP^+ MM1S cells using fluorescence confocal imaging. Bort-NPs induced apoptosis and death in MM1S cells (24 h) (scale bar: 5 μm) (*C*) as measured by Annexin-V/PI flow cytometry; and (*D*) bioluminescent signal quantification of GFP^+Luc^+ MM1S cells (24, 48 h). In *C* and *D*, cells were treated with effective bortezomib concentrations of ∼3.6 or ∼7.3 nM (Bort-NPs) or free drug (5 or 10 nM). *T* tests evaluating efficacy of treatments vs. NP controls at same time point show equivalent efficacy of 7.3 nM Bort-NPs and 10 nM Free Drug. (*E*) Annexin-V/PI flow cytometry of GFP^+ MM1S cells treated with Empty-NPs, Ald-Empty-NPs, ∼3.6 nM Ald-Bort-NPs, and ∼7.3 nM Bort-NPs after 24 h. The stacked bars represent means ± SEM. (*F–I*) Mice injected with GFP^+Luc^+ MM1S cells, treated with Ald-Empty-NPs, Bort-NPs, Free Drug, and Ald-Bort-NPs twice a week, starting at day 21 after tumor cell injection ($n = 7$). (*F*) BLI flux measuring tumor burden in mice from day 21 to 38. (*G*) Quantification of BLI at day 38. (*H*) Survival data for mice treated with Bort-NPs, Ald-Bort-NPs, Free Drug, or NP controls. (*I*) Representative BLI images of mice at day 38 from the four groups. Scale represents luminescence signal from Luc^+ MM1S cells, quantifying tumor burden.

staining and flow cytometry showed similar induction of apoptosis of MM1S cells at 24 h using bortezomib-loaded NPs or free drug (Fig. 3*C*). Bioluminescent quantification of cell numbers also demonstrated similar in vitro bortezomib efficacies when delivered in NPs or as a free drug, with no significant difference found between 7.3 nM Bort-NPs and 10 nM free drug at 48 h. All treatments significantly decreased MM1S cell numbers at all time points. These results illustrate the ability for NPs to effectively deliver bortezomib to inhibit myeloma growth in vitro (Fig. 3*D*). The addition of Ald did not change the efficacy of Bort-NPs in inducing apoptosis, and both drug-free PP and Ald-PP NPs were nontoxic, as expected (Fig. 3*E*) (10, 11).

NPs Inhibit MM Growth in Vivo. In the next set of experiments, we used a MM1S xenograft osteolytic bone disease model (22) where GFP^+Luc^+ MM1S cells were injected into the tail vein of SCID-beige mice, treated with NPs and controls, and measured for tumor burden using bioluminescent imaging (BLI) and survival. MM1S tumor burden was significantly decreased by Ald-Bort-NPs, Bort-NPs (Ald free), and Free Drug compared with Ald-Empty-NPs (no-drug Ald-PP NPs) at day 38 (Fig. 3 *F* and *G*). These data indicate that Ald-Bort-NPs and Bort-NPs were able to reduce tumor burden to the same extent as Free Drug. There was also a significant increase in the survival for mice treated with Ald-Bort-NPs, Bort-NPs, and Free Drug, compared with Ald-Empty-NPs (Fig. 3 *H* and *I*). This evidence demonstrates that bortezomib delivery with NPs works as well as conventional, free drug delivery, in the mice model.

In the treatment study of established myeloma, we believe cancer inhibition was not observed with the use of NPs because, in mice, much of the disease develops outside of the bone marrow niche (circulating and lodged in extramedullary/nonbone locations), which is one of the major differences between mouse myeloma models and the clinical presentation, making inhibition by bortezomib equally efficacious when delivered by any of the compared methods. Conversely, in patients, MM growth is more bone-restricted and treatment with bone-targeting NPs could potentially show increased efficacy vs. free drug or non–bone-targeted NPs by increasing the therapeutic window specifically in the location of the highest MM cell concentration. Furthermore, although we are unable to model peripheral neuropathy in mice due to inherent neurological differences in mice and humans, bone-targeted NPs may potentially improve patient outcomes by decreasing neuropathy from off-target effects of bortezomib.

Bortezomib Increases Osteogenic Differentiation in Vitro and in Vivo. After validating the ability for bortezomib to increase osteogenic differentiation of bone marrow-derived mesenchymal stromal cells (MSCs) in vitro (Fig. S4), we assessed the effects of bortezomib in vivo. Mice were pretreated with Ald-Empty-NPs, Free Drug, or Ald-Bort-NPs for 3 wk, thrice a week, and euthanized thereafter. Bones were analyzed with micro-computed tomography (micro-CT) analysis of femur and tibia, and static bone histomorphometry of the tibia. We observed significantly increased bone trabecular volume, as demonstrated in Von Kossa-stained tibia slides (Fig. 4*A*),

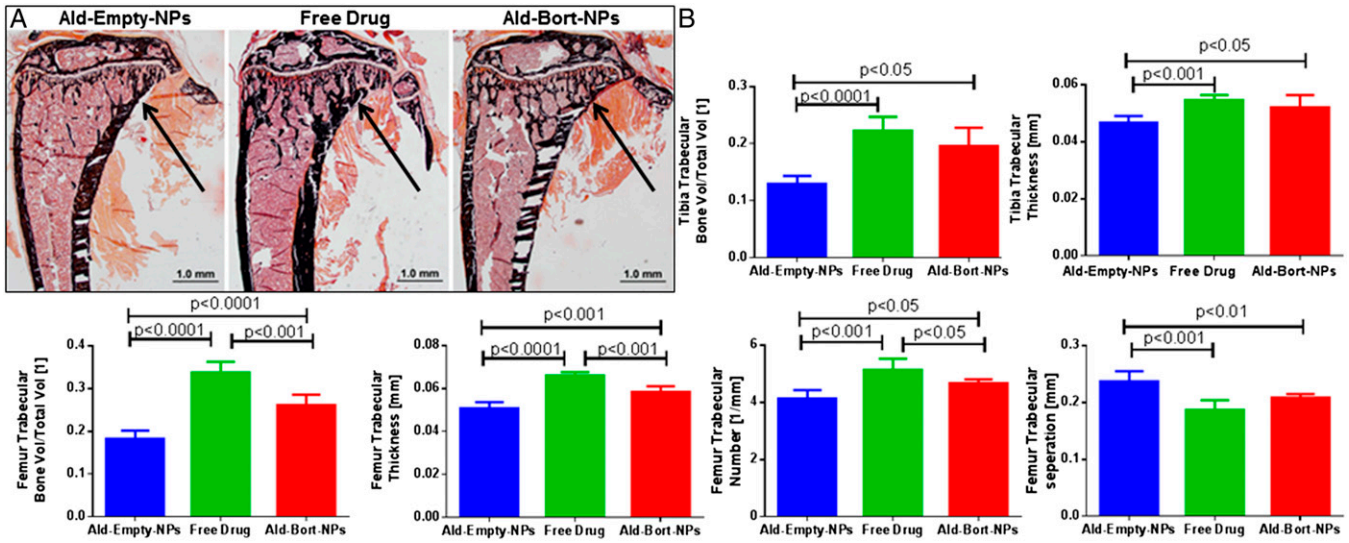

Fig. 4. In vivo effects of bortezomib NPs (single emulsion) on bones. Mice were pretreated for 3 wk, with Ald-Empty-NPs, Free Drug, or Ald-Bort-NPs. Static bone histomorphometry and micro-CT done on these samples show an increase in bone formation markers for the bortezomib-treated groups. (*A*) Representative images from static histomorphometry from each group shown by Von Kossa staining. Trabecular bone volume was increased in Free Drug and Ald-Bort-NP groups compared with that of Ald-Empty-NP group, as indicated by arrows. (*B*) Micro-CT analysis demonstrated significantly higher bone in Ald-Bort-NPs and Free Drug compared with that of Ald-Empty-NPs in terms of the following: tibia trabecular bone volume per total volume, tibia trabecular thickness, femur trabecular bone volume per total volume, femur trabecular thickness, femur trabecular number, and femur trabecular separation.

and quantified with micro-CT in the tibia and femur and histomorphometry of the proximal tibia (Fig. 4*B*). Histomorphometric analysis also demonstrated significant increases in osteoid thickness and decreases in several bone resorption parameters in mice treated with either Ald-Bort-NPs or Free Bortezomib, vs. Ald-Empty-NPs (Table S1), with both changes (increased osteoblastic activity and decreased osteoclastic activity) contributing to the increased bone volume. Significantly higher bone metrics were also observed in Ald-Bort-NPs and Free Drug compared with Ald-Empty NPs using micro-CT quantification, in terms of tibia trabecular bone volume per total volume, tibia trabecular thickness, and femur trabecular bone volume per total volume, femur trabecular thickness, femur trabecular number, and femur trabecular separation (Fig. 4*B*). This evidence demonstrates the ability for both free bortezomib and bortezomib-loaded NPs to increase volume of bone, and number of trabeculae, in vivo over a 3-wk pretreatment period. We next investigated the consequences of these treatments on the growth of MM.

Pretreatment with Bone-Targeted, Bortezomib NPs Inhibits Myeloma Growth. To examine whether modulating the bone marrow niche before metastasis occurs can prevent/delay disease progression, mice were pretreated with Ald-Bort-NPs, Ald-Empty-NPs, or Free Drug for 3 wk, thrice a week. This allowed for the modulation of the bone microenvironment before the arrival of cancer cells. They were then injected with GFP^+Luc^+ MM1S cells into the tail vein and assessed for tumor progression. Of great importance was our observation that pretreatment with Ald-Bort-NP significantly inhibited myeloma growth as observed with significantly lower BLI signal compared with the Free Drug and Ald-Empty-NP groups ($P < 0.05$) (Fig. 5 *A* and *C*). Survival time was also significantly increased in the Ald-Bort-NP group with median survival of 41 d,

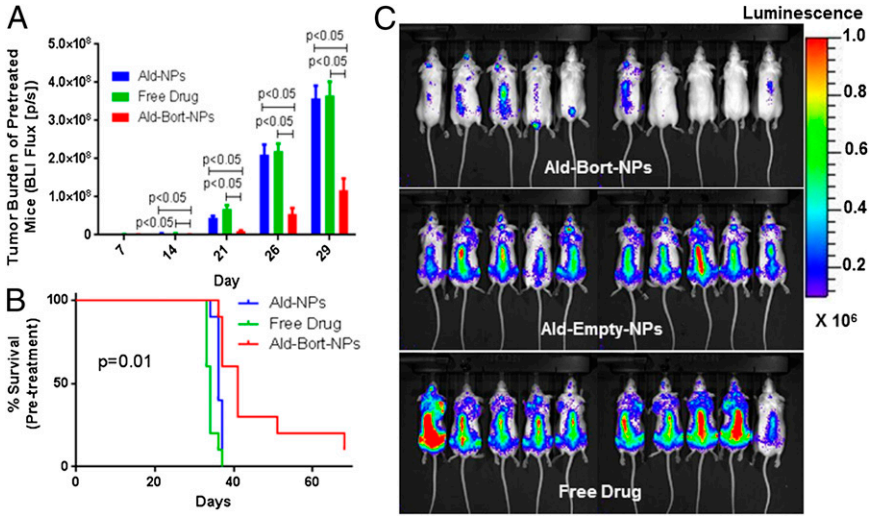

Fig. 5. Pretreatment with Ald-Bort-NPs inhibits myeloma growth better than free drug. (*A*–*C*) Mice were pretreated for 3 wk with Ald-Empty-NPs, Free Drug, or Ald-Bort-NPs and then injected with GFP^+ Luc^+ MM1S cells. (*A*) BLI flux from mice was significantly lower in Ald-Bort-NPs compared with that of Ald-Empty-NPs or Free Drug groups at every day of imaging. (*B*) Survival was also significantly increased in the Ald-Bort-NP–pretreated mice ($P = 0.01$). (*C*) Day 29 images of BLI signal from mice illustrates the reduction of tumor burden in mice pretreated with Ald-Bort-NPs ($n = 10$).

compared with just 34 or 36 d in the Free Drug group, and Ald-Empty-NP groups, respectively (Fig. 5*B*). In a second in vivo study (Fig. S5), we confirmed that pretreatment with bone-homing bortezomib NPs improved survival compared with pretreatment with nontargeted bortezomib NPs. Both treatments significantly improved survival compared with empty-NPs, further confirming that bortezomib NP drug delivery creates a less hospitable bone microenvironment for cancer cells. These results suggests that Ald-Bort-NPs may have the ability to alter the microenvironment to prevent myeloma growth via mechanisms other than increasing in bone volume, trabecular number, or osteoid thickness, and should be explored for their ability to inhibit other bone-metastatic cancers.

Conclusion

In summary, we developed, biodegradable polymeric NPs capable of targeting bone and delivering the payload in a spatiotemporally controlled manner. These NPs were shown to enhance bone homing due to long circulation and bone mineral-targeting capabilities. The bone-targeted NPs with sustained release polymer technology delivered bortezomib to bone marrow microenvironment specifically, to produce the antimyeloma effects similar to a free drug. However, the major drawback of using a free drug, bortezomib, is peripheral neuropathy (5), and the use of our NPs would be hugely beneficial by enabling bone-specific drug delivery, which should drastically decrease these side effects in patients. It is also well known that MM resistance is due to cell dormancy within the bone marrow, and the clonal nature of MM, which is driven by a wide range of interactions, constantly evolving mutations, and heterogeneous abnormalities. However, targeting the microenvironment, on the other hand, translates well to all patients, regardless of the driver mutation. Thus, our NPs, which are specifically designed to home to the bone marrow, release the drug to target both the cancer and the microenvironmental cells. Furthermore, the design of our engineered NP has far-reaching advantages of flexibility of NP design, scalability, biocompatibility and biodegradability, long circulation, sustained drug release, bone-homing property, and fine-tuned components for clinical translation. In the future, this platform could be used in many other cancer models to deliver many different anticancer agents. The results of the present work demonstrate the tremendous potential of the bone-targeted Ald-PP NPs in the pretreatment strategy for modifying the bone microenvironment with suitable drugs to prevent cancer progression and lesion formation, providing a promising nanomedicine approach for MM therapy.

Materials and Methods

(See *SI Materials and Methods* for details.) To optimize NP formulation with suitable physicochemical characteristics, with varying ratios of target ligand (Ald) to PEG density on NP surface, and to maximize the drug load, we prepared a library of NPs, using different polymer molecular weights, blending different ratios of synthesized polymers (Figs. S1 and S2) (23), using different formulation techniques, and varying the conditions of formulations. The affinity of Ald-conjugated NPs (Ald-PP) toward bone mineral (HA) was investigated in comparison with nontargeted (PP) NPs. We studied the in vivo biodistribution of $Alexa_{647}$-labeled Ald-PP NPs with whole-mouse imaging. NPs were injected i.p. and after imaging (1, 24 h), the mouse bones were dissected, sectioned, and imaged for investigation of bone homing of labeled NPs (Fig. S3). We investigated the in vitro efficacy of Bort-NPs by measuring apoptosis via flow cytometry, and bioluminescence assay, where empty NPs, and free bortezomib were the controls (24). The in vivo efficacy studies used female Nod/SCID beige mice in treatment or pretreatment regimes. For treatment studies, mice injected with Luc^+/GFP^+ MM1S cells were randomly divided into four groups ($n = 7$). After injecting cancer cells, on day 21 mice were injected (i.p.) twice a week with 0.5 mg/kg bortezomib (or with an equivalent amount of Ald-Empty-NPs): Ald-Empty-NPs, Free Drug (bortezomib), Ald-Bort-NPs, and nontargeted Bort-NPs, and were imaged twice a week. In the case of NP pretreatment regime, female Nod/SCID beige mice were randomized into three groups ($n = 10$) and injected (i.p.) thrice a week for 3 wk, with 0.3 mg/kg bortezomib or with an equivalent amount of Ald-Empty-NPs. The pretreatment groups were as follows: Ald-Bort-NPs, Free Drug, and Ald-Empty-NPs in study 1 and Ald-Bort-NPs, Ald-Empty-NPs, and Nontargeted Bort-NPs in study 2. After 3 wk, the mice were injected with Luc^+GFP^+ MM1S cell. BLI was performed weekly on these mice and survival was assessed. Additionally, an ex vivo micro-CT analysis and static histomorphometry (25) of mouse bones (femur, tibia, and fibula) were performed after a 3-wk pretreatment period to validate bortezomib-induced increase in osteogenesis. See *SI Materials and Methods, Statistical Analysis* for the details of the statistical analysis.

ACKNOWLEDGMENTS. This work was supported by Department of Defense Grant W81XWH-05-1-0390; National Institutes of Health Grants R00 CA160350, R01 FD003743, R01 CA154648, and CA151884; Movember–Prostate Cancer Foundation Challenge Award; National Research Foundation of Korea K1A1A2048701; and the David Koch–Prostate Cancer Foundation Award in Nanotherapeutics. N.B. acknowledges Canadian Institutes of Health Research.

1. Roodman GD (2009) Pathogenesis of myeloma bone disease. *Leukemia* 23(3):435–441.
2. Reagan MR, Ghobrial IM (2012) Multiple myeloma mesenchymal stem cells: Characterization, origin, and tumor-promoting effects. *Clin Cancer Res* 18(2):342–349.
3. Coleman RE (2001) Metastatic bone disease: Clinical features, pathophysiology and treatment strategies. *Cancer Treat Rev* 27(3):165–176.
4. Garrett IR, et al. (2003) Selective inhibitors of the osteoblast proteasome stimulate bone formation in vivo and in vitro. *J Clin Invest* 111(11):1771–1782.
5. Ozaki S, et al. (2007) Therapy with bortezomib plus dexamethasone induces osteoblast activation in responsive patients with multiple myeloma. *Int J Hematol* 86(2): 180–185.
6. Giuliani N, et al. (2007) The proteasome inhibitor bortezomib affects osteoblast differentiation in vitro and in vivo in multiple myeloma patients. *Blood* 110(1):334–338.
7. Heider U, et al. (2006) Bortezomib increases osteoblast activity in myeloma patients irrespective of response to treatment. *Eur J Haematol* 77(3):233–238.
8. Zangari M, et al. (2005) Response to bortezomib is associated to osteoblastic activation in patients with multiple myeloma. *Br J Haematol* 131(1):71–73.
9. Terpos E, et al. (2010) Increased bone mineral density in a subset of patients with relapsed multiple myeloma who received the combination of bortezomib, dexamethasone and zoledronic acid. *Ann Oncol* 21(7):1561–1562.
10. Hrkach J, et al. (2012) Preclinical development and clinical translation of a PSMA-targeted docetaxel nanoparticle with a differentiated pharmacological profile. *Sci Transl Med* 4(128):128ra39.
11. Kamaly N, Xiao Z, Valencia PM, Radovic-Moreno AF, Farokhzad OC (2012) Targeted polymeric therapeutic nanoparticles: Design, development and clinical translation. *Chem Soc Rev* 41(7):2971–3010.
12. Swami A, et al. (2012) *Multifunctional Nanoparticles for Drug Delivery Applications*, eds Svenson S, Prud'homme RK (Springer, Boston), pp 9–29.
13. Zhang X-Q, et al. (2012) Interactions of nanomaterials and biological systems: Implications to personalized nanomedicine. *Adv Drug Deliv Rev* 64(13):1363–1384.
14. Zhang S, Gangal G, Uludağ H (2007) "Magic bullets" for bone diseases: Progress in rational design of bone-seeking medicinal agents. *Chem Soc Rev* 36(3):507–531.
15. Sayed D, Al-Sadoon MK, Badr G (2012) Silica nanoparticles sensitize human multiple myeloma cells to snake (*Walterinnesia aegyptia*) venom-induced apoptosis and growth arrest. *Oxid Med Cell Longev* 2012:386286.
16. Ravindran J, et al. (2010) Thymoquinone poly (lactide-co-glycolide) nanoparticles exhibit enhanced anti-proliferative, anti-inflammatory, and chemosensitization potential. *Biochem Pharmacol* 79(11):1640–1647.
17. Sou K, Oyajobi B, Goins B, Phillips WT, Tsuchida E (2009) Characterization and cytotoxicity of self-organized assemblies of curcumin and amphiphatic poly(ethylene glycol). *J Biomed Nanotechnol* 5(2):202–208.
18. Taylor CA, et al. (2012) Modulation of eIF5A expression using SNS01 nanoparticles inhibits NF-κB activity and tumor growth in murine models of multiple myeloma. *Mol Ther* 20(7):1305–1314.
19. Yang C, et al. (2013) Paclitaxel-Fe_3O_4 nanoparticles inhibit growth of CD138(–) CD34 (–) tumor stem-like cells in multiple myeloma-bearing mice. *Int J Nanomedicine* 8: 1439–1449.
20. Maillard S, et al. (2005) Innovative drug delivery nanosystems improve the anti-tumor activity in vitro and in vivo of anti-estrogens in human breast cancer and multiple myeloma. *J Steroid Biochem Mol Biol* 94(1-3):111–121.
21. Cirstea D, et al. (2010) Dual inhibition of akt/mammalian target of rapamycin pathway by nanoparticle albumin-bound-rapamycin and perifosine induces antitumor activity in multiple myeloma. *Mol Cancer Ther* 9(4):963–975.
22. Azab AK, et al. (2009) CXCR4 inhibitor AMD3100 disrupts the interaction of multiple myeloma cells with the bone marrow microenvironment and enhances their sensitivity to therapy. *Blood* 113(18):4341–4351.
23. Pridgen EM, et al. (2013) Transepithelial transport of fc-targeted nanoparticles by the neonatal fc receptor for oral delivery. *Sci Transl Med* 5(213):213ra167.
24. Leleu X, et al. (2007) The Akt pathway regulates survival and homing in Waldenstrom macroglobulinemia. *Blood* 110(13):4417–4426.
25. Dempster DW, et al. (2013) Standardized nomenclature, symbols, and units for bone histomorphometry: A 2012 update of the report of the ASBMR Histomorphometry Nomenclature Committee. *J Bone Miner Res* 28(1):2–17.